arXiv:1610.01813v1 [physics.optics] 6 Oct 2016

Anderson localisation and optical-event horizons in rogue-soliton generation

Mohammed F. Saleh,[1,2] Claudio Conti,[3,4] and Fabio Biancalana[1]

[1] *Scottish Universities Physics Alliance (SUPA), Institute of Photonics and Quantum Sciences, Heriot-Watt University, EH14 4AS Edinburgh, UK*
[2] *Department of Mathematics and Engineering Physics, Alexandria University, Alexandria, Egypt*
[3] *Department of Physics, University Sapienza, Piazzale Aldo Moro 2, 00185 Rome, Italy*
[4] *Institute for Complex Systems (ISC-CNR), Via dei Taurini 19, 00185 Rome, Italy*

(Dated: October 7, 2016)

We show that the true origin of rogue solitons in optical fibres is due to the combined action of linear Anderson localisation and the formation of optical-event horizons. Anderson localised modes are formed in certain temporal locations due to the random background noise. Such localised modes seed the formation of solitary waves at those preferred locations, while the strongest Anderson mode generates the rogue soliton. The event horizon effect between dispersive waves and solitons produces an artificial collective acceleration that favours the collision of solitons during the rogue wave formation.

I. INTRODUCTION

Modulational instability (MI) is one of the most basic and important nonlinear optical processes. In optical fibers, MI induces spectral sidebands in narrowband optical pulses, eventually leading to a broad supercontinuum after propagation of a few nonlinear lengths [1–7]. Photonic crystal fibres (PCFs) strongly can enhance the supercontinuum generation by dispersive landscape optimization and strong light confinement [8–10]. Generation of supercontinua using long pulses, in comparison to ultrashort pulses, lacks coherence and stability, mainly because of the amplification of the background noise [11]. Nevertheless, the understanding of the influence of the input noise on the output spectrum has driven multiple studies [12–15]. The evidence presented by Solli *et al.* that the output spectra contain statistically rare rogue events with large intensities and enhanced redshift [16–23] boosted huge interest because of the interesting connections of this phenomenon with rare destructive rogue-waves in oceans [24, 25]. In optical rogue events, the interplay between nonlinearity and dispersion amplifies the background noise breaking the pulse via soliton fission [26]. Because of the Raman nonlinearity, solitons are continuously redshifted and decelerate in the time domain [27, 28]. Depending on the specific initial input noise, a rogue soliton with very large intensity may appear inside the fibre during the spatial propagation of the pulse.

In this Letter, we propose a novel groundbreaking perspective of this process. We show here that Anderson localisation [29] and optical event horizons [30] are the main ingredients for rogue soliton generation by MI. Our study provides a clear explanation of how noise drives the dynamics of 'freak' optical waves. The reported concepts will also be important for a variety of related fields, governed by similar models, such as ocean wave physics, and Bose-Einstein Condensates.

II. GENERALIZED NONLINEAR SCHRÖDINGER EQUATION AND ANDERSON LOCALISATION

In 1958 Philip Anderson reported that disorder can induce localized states, due to the cumulative effects of multiple scatterings, a phenomenon known today as Anderson localisation [29]. In optics, disorder-induced transverse localisation has been demonstrated in mm-long photonic lattices [31–37]. Various authors also reported on the related effect of nonlinearity on Anderson localisation [32, 38–43]. Here we consider the temporal counterpart of these studies. Using the slowly-varying envelope (SVE) approximation, the propagation of intense pulses in optical fibres is governed by the generalized nonlinear Schrödinger equation [44],

$$\left[i\partial_z + \hat{D}(i\partial_t) + \gamma\left(1 + i\tau_{sh}\partial_t\right)\left(R(t) \otimes |A(z,t)|^2\right)\right] A = 0, \tag{1}$$

where t is the time in a reference frame moving with the pulse group velocity, $\hat{D} = \sum_{m\geq 2} \beta_m (i\partial_t)^m / m!$ is the dispersion operator, β_m, γ, τ_{sh} are the dispersion, nonlinear and self-steepening coefficients, respectively, $R(t)$ is the nonlinear response function that includes Kerr and Raman contributions, $\otimes$ denotes the convolution integral, $\gamma = n_2\omega_0/cA_{\text{eff}}$, n_2 is the nonlinear refractive in units of m^2/W, ω_0 is the pulse central frequency, c is the speed of light in vacuum, and A_{eff} is the effective optical mode area. Neglecting higher-order nonlinear and dispersion coefficients, Eq. (1) becomes simply

$$i\partial_z A - \frac{\beta_2}{2}\partial_t^2 A + \frac{\omega_0}{c}\Delta n(z,t)A = 0, \tag{2}$$

where the nonlinear-Kerr term results in a pure temporal modulation of the refractive index $\Delta n(z,t) = n_2|A|^2/A_{\text{eff}}$, which will follow the variation of the pulse intensity during propagation in z. The SVE approximation implies that $\Delta n(z,t) \approx \Delta n(t)$ over a short propagation distance. In these spatial z-intervals the random temporal variation Eq.(2) due to the input noise acts

like a transverse disorder and induces localized states. Optical fibres are usually meters long and the complex envelope varies slowly over centimeters or meters range (i.e. various orders of magnitude more than the length of the waveguides used in Anderson localisation experiments [32]). Therefore, light pulses are *temporally* localised in different locations during the propagation along z for any specific noise realization (Fig. 1a).

III. LOCALIZED ANDERSON MODES IN TEMPORAL POTENTIALS

Strong pulses induce temporal potentials during propagation in optical fibres via Kerr nonlinearity. These potentials will sustain linear modes that follow the track of the pulse. In the case of a long intense pulse, its amplitude is susceptible to the input shot noise. This produces a random temporal modulation of the refractive index, resulting in an evolving 1D random potential. The temporally localized states solutions of this structure follow the linear Schrödinger equation,

$$i\partial_z u - \frac{\beta_2}{2}\partial_t^2 u + \frac{\omega_0}{c}\Delta n(z,t)u = 0, \tag{3}$$

where u is the complex mode amplitude. Expressing $u(z,t) = f(t)\exp(i\lambda z)$, Eq. (3) becomes an eigenvalue problem with f and λ representing the eigenfunctions and eigenvalues, respectively. The localisation time $T_{\rm loc}$ for the ground state is given by [39]:

$$T_{\rm loc}(z) = \frac{\left(\int |f(z,t)|^2\, dt\right)^2}{\int |f(z,t)|^4\, dt}. \tag{4}$$

As a practical example, we consider the propagation of a long superGaussian pulse with central wavelength 1060 nm, full-width-half-maximum (FWHM) 7 ps and input power 100 W in a solid silica-core photonic crystal fibre with zero-dispersion wavelength located at 1055 nm. We follow Ref. [17] for the values of higher-order dispersion, Kerr nonlinearity and self-steepening coefficients. A superGaussian pulse induces a quasi step-index temporal waveguide. In our numerical analysis, we first switch off higher-order dispersion terms and all the nonlinear effects apart from the Kerr nonlinearity (Raman effect and self-steepening) in order to understand the role of the noise. Figure 1(a,b) show the temporal evolution of the nonlinear pulse and the onset of the ground state localized mode, respectively. Panel (c) depicts the corresponding $z-$evolution of the eigenvalue and the localisation time given by Eq. (4). Starting from $z = 0$, the background noise builds up and then alters the pulse amplitude around $z = 6$ m due to MI.

Discretising the optical fibre into small segments, one can observe clearly different localization positions of the

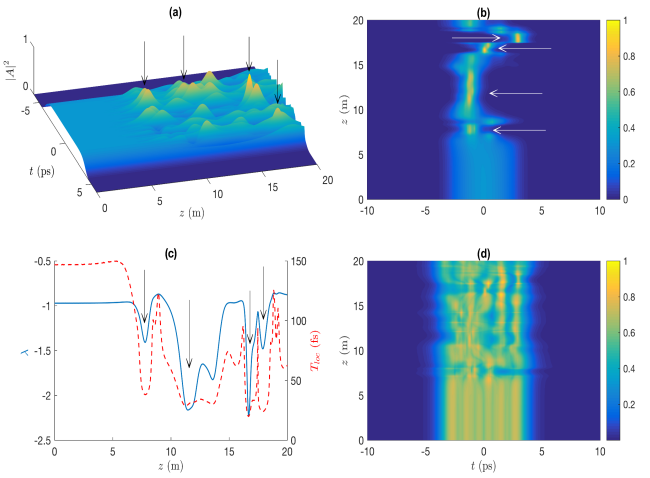

FIG. 1. (Color online). (a) Temporal evolution of a super-Gaussian pulse $A = \exp\left[-1/2\,(t/T_0)^{10}\right]$ at wavelength 1060 nm, with $T_0 = 3.63$ ps (FWHM = 7 ps) and input power 100 W inside the solid silica-core photonic crystal fibre of Ref. [17] in the absence of higher-order dispersion, Raman effect and self-steepening. (b) Temporal evolution of the ground Anderson state of the induced temporal-waveguide. The arrows in (a,b) point out solitonization of Anderson localisation phenomenon. (c) Spatial evolution of the eigenvalue and localisation time of the fundamental Anderson mode. The arrows indicate positions where the eigenvalue and localisation time are suppressed. (d) Temporal evolution of the first five states.

lowest energy Anderson mode. These positions are indicated by the arrows in Figs. 1(b,c). The track of the fundamental Anderson mode is disrupted multiple times, since each segment of the fibre is considered as a different random system. Interestingly, the pulse experiences an amplification at the positions where Anderson localisation occurs, a phenomenon known as solitonisation of Anderson localisation [39], as indicated by the arrows in Fig. 1(a). This is also accompanied by a reduction of the eigenvalue of the fundamental Anderson mode as shown by the arrows in panel (c), since the soliton amplitude is proportional to $|\lambda|$. The strongest localisation occurs at $z = 16.7$ m. In panel (d), we show the first five Anderson modes. When MI takes place, these modes acts as seeds and emit solitons that get further compressed over short propagation distances via the Anderson localisation.

IV. OPTICAL-EVENT HORIZON

Optical-event horizons are also playing a major role in rogue-soliton generation [30]. The nonlinear temporal waveguide due to a strong pulse in a Kerr medium acts as an optical analogue of a white-hole event horizon. A trailing probe pulse with slightly higher group velocity cannot penetrate the white-hole analogue and bounces back [30]. Because of cross-phase modulation the probe

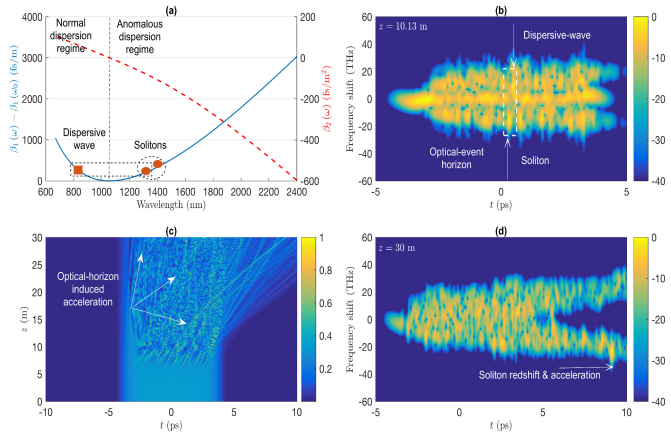

FIG. 2. (Color online). (a) β_1 and β_2 Vs wavelength. The dotted rectangle shows a group of a soliton and a dispersive-wave with nearly group velocities. The dotted circle shows a group of solitons with nearly group velocities. In the presence of the second and third-order dispersion coefficients, and Kerr nonlinearity: (b) XFROG representation of the super-Gaussian pulse at $z = 10.13$ m; (b) Temporal evolution of the superGaussian pulse; (d) XFROG representation at $z = 30$ m. XFROG contour plots are given in a logarithmic scale and truncated at -40 dB.

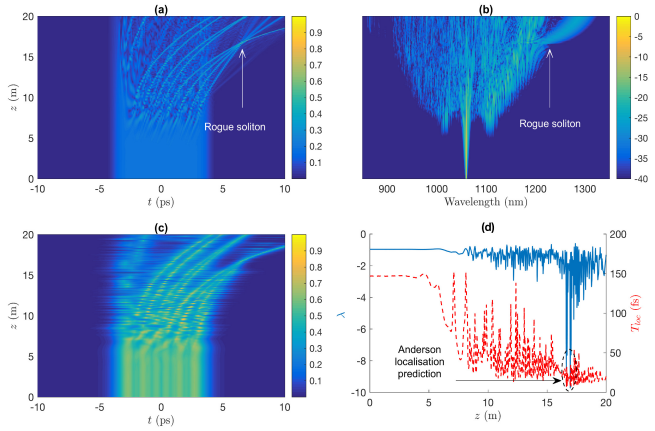

FIG. 3. (Color online). (a,b) Temporal and spectral evolution of the superGaussian pulse taking into account all the linear and nonlinear effects. (c) Temporal evolution of the first five Anderson modes of the induced temporal-waveguide. (d) The spatial dependency of the eigenvalue and localisation time of the fundamental mode. The spectral contour plot is given in a logarithmic scale and truncated at -40 dB. Temporal contour plots are normalised to their peaks.

speed slows down until it matches the strong pulse velocity. This effect can induce octave-spanning highly-coherent supercontinua [45, 46], and soliton interactions mediated by trapped dispersive waves [47, 48]. Rogue events in the group velocity horizon due to soliton and dispersive waves interactions have been also considered [49, 50].

Third-order dispersion in Eq. (2) will force solitons to emit dispersive waves. A large pool of solitons and dispersive waves will form after MI amplifies the background noise. Near the zero dispersion wavelength, the concave group-velocity β_1 dispersion (Fig. 2(a)) enables synchronous co-propagation of solitons and dispersive waves in the anomalous and normal dispersive regimes, respectively. Hence, the condition for the optical group-velocity event horizon [30] between a leading soliton and a trailing dispersive wave can be easily satisfied. This is evident in the cross frequency optical gating spectrogram (XFROG) at $z = 10.13$ m in Fig. 2(b). In this case, the soliton acts as a white hole, through which the dispersive wave can not flow. The soliton barrier reflects back the dispersive wave after collision. Interestingly, the collision can result in a soliton self-frequency redshift accompanied by a deceleration in the time domain even in the absence of Raman nonlinearity. Panels (c,d) in Fig. 2 show the temporal evolution of the pulse inside the fibre and the XFROG at the fibre end. A soliton at the leading edge of the pool experiences greater acceleration than one at the trailing edge; indeed the former undergoes many collisions.

The third-order dispersion induces a rapid evolution of the background noise, and shortens the longitudinal distance where Anderson localisation can take place to a few centimetres. This is accompanied by a rapid change in the eigenvalue and localisation time of the fundamental Anderson mode in comparison to Fig. 1(c). We have found that the inclusion of higher-order dispersion coefficients $\beta_{m>3}$ and self-steepening effects τ_{sh} does not involve additional features in pulse dynamics, other than fostering the randomness of the temporal potential.

V. ROGUE-SOLITON GENERATION

Figure 3(a,b) displays the temporal and spectral evolution of the superGaussian pulse with Raman effect producing strong soliton self-frequency redshift and deceleration in the time domain. Initially, the amplitude of the pulse is uniform, hence, a rectangular potential well is formed with defined linear Anderson modes. MI causes the potential to fluctuate randomly, and solitons are emitted within the potential dips. The linear Anderson modes of the random system are seeds for the soliton emissions as shown in panel (c); remarkably this plot shows clearly the solitonic tracks without the background noise. Initially, the emitted solitons have similar amplitudes and accelerations, since the seeding linear Anderson modes have very close eigenvalues. This results in initial frequent hopping of the position of the fundamental Anderson mode with any slight perturbation and will disfavour any soliton–soliton collisions. However at every step in the spatial propagation, Anderson localisation randomly amplifies and temporally localises the different solitons. Also, collisions between solitons and dis-

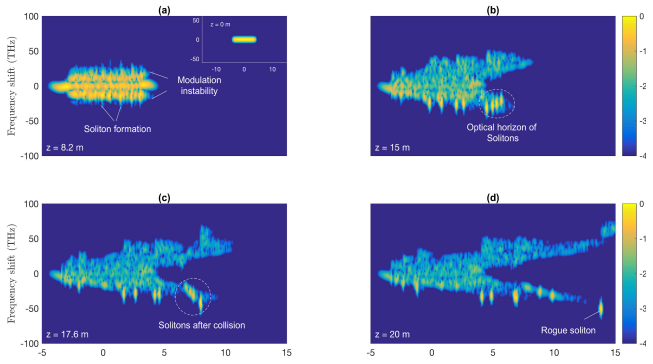

FIG. 4. (Color online). (a-d) XFROG representation of the superGaussian pulse taking into account all the linear and nonlinear effects at different positions along the fibre. The inset in (a) is XFROG at $z = 0$. Contour plots are given in a logarithmic scale and truncated at -40 dB.

persive waves in the normal dispersion regime will induce the optical-event horizon acceleration that is stronger for solitons at the leading edge of the pulse. This results in solitons having different accelerations, and so they become more and more likely to collide.

Soliton collisions occur when their trajectories intersect, however, specific collisions lead to rogue solitons with large amplitude and frequency redshift. The specific collisions are due to further optical-event horizons that arise by the interaction of two or more solitons. Consider a scenario between two solitons with similar amplitudes and similar frequencies. The Raman-induced soliton acceleration is an additional factor, which affects the solitons group velocities, beside the dispersion. At some point inside the fibre, the two solitons are locked together via matching their group velocities, and an optical-event horizon between the two solitons is formed with long nonlinear interaction length. Figure 4 shows the XFROG representation at different positions inside the fibre. MI and soliton formation are shown in panel (a). Because of Raman nonlinearity, solitons approach in frequency and time [panel (b)] and accumulate at the optical-horizon. The resulting collisions form a rogue soliton [panel (c)]. Panel (d) shows the rogue soliton after the strong redshift in propagation. The collisions are inelastic because the amplitudes of the solitons reduces, as in Fig. 3(a). Remarkably, the generated rogue soliton position coincides with that predicted by the strongest Anderson localisation, which is $z = 16.7$ m. At the rogue soliton formation, we observe a strong drop of the eigenvalue and localisation time of the fundamental Anderson mode as shown in Fig. 3(d).

VI. CONCLUSIONS

We have found that the true origin of rogue solitons in optical fibres is due to the combined action of Anderson localisation and horizon effects. Solitons that appear from nowhere during propagation stem from linear Anderson localisations of the random temporal potential of a strong pulse, before this pulse breaks due to MI. Anderson localisation enhances the intensity of the solitons and reduces their temporal widths in a few centimetres of propagation. After this 'solitonisation of the Anderson localisation', third-order dispersion generates dispersive waves. The interaction of the dispersive waves with the optical horizons results in soliton deceleration even when Raman nonlinearity is absent. Clusters of solitons form mutual optical horizons, leading to a rogue emission at a position predicted by the original strongest Anderson localisation. These rich mechanisms demonstrate the complexity underlying rogue soliton generation and furnish a clear evidence of the previously-unconsidered temporal Anderson localisation, and the unexpected interaction with optical horizons. This scenario may potentially lead to novel routes for the control of extreme nonlinear waves via linear-disorder optimisation.

We believe that our findings solve one of the most debated questions in the field, namely: are rogue waves generated by processes that are intrinsically linear or nonlinear? The answer to this question is that a linear process, Anderson localisation, seeds localised structures from noise, and subsequently a nonlinear phenomenon, the solitonisation of Anderson localisation, together with optical-event horizons induce the last steps of rogue soliton formation.

Acknowledgments — MFS would like to acknowledge the support of his research by Royal Society of Edinburgh and Scottish Government.

[1] S. Coen, A. H. L. Chau, R. Leonhardt, J. D. Harvey, J. C. Knight, W. J. Wadsworth, and P. S. J. Russell, Opt. Lett. **26**, 1356 (2001).
[2] L. Provino, J. M. Dudley, H. Maillotte, N. Grossard, R. S. Windeler, and B. J. Eggleton, Electronics Letters **37**, 558 (2001).
[3] A. V. Avdokhin, S. V. Popov, and J. R. Taylor, Opt. Lett. **28**, 1353 (2003).
[4] T. Schreiber, J. Limpert, H. Zellmer, A. Tnnermann, and K. Hansen, Optics Communications **228**, 71 (2003).
[5] W. J. Wadsworth, N. Joly, J. C. Knight, T. A. Birks, F. Biancalana, and P. S. J. Russell, Opt. Express **12**, 299 (2004).
[6] F. Vanholsbeeck, S. Martin-Lopez, M. González-Herráez, and S. Coen, Opt. Express **13**, 6615 (2005).
[7] M. H. Frosz, O. Bang, and A. Bjarklev, Opt. Express **14**, 9391 (2006).

[8] J. C. Knight, Nature **424**, 847 (2003).
[9] P. Russell, Science **299**, 358 (2003).
[10] P. S. Russell, J. Lightwave Technol. **24**, 4729 (2006).
[11] J. M. Dudley, G. Genty, and S. Coen, Rev. Mod. Phys. **78**, 1135 (2006).
[12] N. R. Newbury, B. R. Washburn, K. L. Corwin, and R. S. Windeler, Opt. Lett. **28**, 944 (2003).
[13] S. M. Kobtsev and S. V. Smirnov, Opt. Express **14**, 3968 (2006).
[14] A. Demircan and U. Bandelow, Applied Physics B **86**, 31 (2006).
[15] D. Tuürke, S. Pricking, A. Husakou, J. Teipel, J. Herrmann, and H. Giessen, Opt. Express **15**, 2732 (2007).
[16] D. R. Solli, C. Ropers, P. Koonath, and B. Jalali, Nature **450**, 1054 (2007).
[17] J. M. Dudley, G. Genty, and B. J. Eggleton, Opt. Express **16**, 3644 (2008).
[18] G. Genty, C. de Sterke, O. Bang, F. Dias, N. Akhmediev, and J. Dudley, Physics Letters A **374**, 989 (2010).
[19] R. Driben and I. Babushkin, Opt. Lett. **37**, 5157 (2012).
[20] P. T. S. DeVore, D. R. Solli, D. Borlaug, C. Ropers, and B. Jalali, Journal of Optics **15**, 064001 (2013).
[21] J. M. Dudley, F. Dias, M. Erkintalo, and G. Genty, Nat Photon **8**, 755 (2014).
[22] A. Armaroli, C. Conti, and F. Biancalana, Optica **2**, 497 (2015).
[23] J. M. Soto-Crespo, N. Devine, and N. Akhmediev, Phys. Rev. Lett. **116**, 103901 (2016).
[24] C. Kharif and E. Pelinovsky, European Journal of Mechanics - B/Fluids **22**, 603 (2003).
[25] A. R. Osborne, *Nonlinear Ocean Waves and the Inverse Scattering Transform* (Academic Press, 2010).
[26] Y. Kodama and A. Hasegawa, IEEE Journal of Quantum Electronics **23**, 510 (1987).
[27] E. M. Dianov, A. Ya. Karasik, P. V. Mamyshev, A. M. Prokhorov, V. N. Serkin, M. F. Stel'makh, and A. A. Fomichev, JETP Lett. **41**, 294 (1985).
[28] F. M. Mitschke and L. F. Mollenauer, Opt. Lett. **11**, 659 (1986).
[29] P. W. Anderson, Phys. Rev. **109**, 1492 (1958).
[30] T. G. Philbin, C. Kuklewicz, S. Robertson, S. Hill, F. König, and U. Leonhardt, Science **319**, 1367 (2008).
[31] H. De Raedt, A. Lagendijk, and P. de Vries, Phys. Rev. Lett. **62**, 47 (1989).
[32] T. Schwartz, G. Bartal, S. Fishman, and M. Segev, Nature **446**, 52 (2007).
[33] Y. Lahini, A. Avidan, F. Pozzi, M. Sorel, R. Morandotti, D. N. Christodoulides, and Y. Silberberg, Phys. Rev. Lett. **100**, 013906 (2008).
[34] Y. Lahini, R. Pugatch, F. Pozzi, M. Sorel, R. Morandotti, N. Davidson, and Y. Silberberg, Phys. Rev. Lett. **103**, 013901 (2009).
[35] A. Szameit, Y. V. Kartashov, P. Zeil, F. Dreisow, M. Heinrich, R. Keil, S. Nolte, A. Tünnermann, V. Vysloukh, and L. Torner, Opt. Lett. **35**, 1172 (2010).
[36] L. Levi, M. Rechtsman, B. Freedman, T. Schwartz, O. Manela, and M. Segev, Science **332**, 1541 (2011).
[37] M. Segev, Y. Silberberg, and D. N. Christodoulides, Nat Photon **7**, 197 (2013).
[38] C. Conti and A. Fratalocchi, Nat Phys **4**, 794 (2008).
[39] C. Conti, Phys. Rev. A **86**, 061801 (2012).
[40] R. G. S. El-Dardiry, S. Faez, and A. Lagendijk, Phys. Rev. B **86**, 125132 (2012).
[41] M. Leonetti, S. Karbasi, A. Mafi, and C. Conti, Phys. Rev. Lett. **112**, 193902 (2014).
[42] M. Leonetti, S. Karbasi, A. Mafi, and C. Conti, Applied Physics Letters **105** (2014), 10.1063/1.4900781.
[43] M. Leonetti, S. Karbasi, A. Mafi, and C. Conti, Nat Commun **5** (2014).
[44] G. P. Agrawal, *Nonlinear Fiber Optics*, 4th ed., San Diego, California (Academic Press, 2007).
[45] A. Demircan, S. Amiranashvili, C. Brée, and G. Steinmeyer, Phys. Rev. Lett. **110**, 233901 (2013).
[46] A. Demircan, S. Amiranashvili, C. Brée, U. Morgner, and G. Steinmeyer, Opt. Express **22**, 3866 (2014).
[47] A. V. Yulin, R. Driben, B. A. Malomed, and D. V. Skryabin, Opt. Express **21**, 14481 (2013).
[48] I. Oreshnikov, R. Driben, and A. V. Yulin, Opt. Lett. **40**, 4871 (2015).
[49] A. Demircan, S. Amiranashvili, and G. Steinmeyer, Phys. Rev. Lett. **106**, 163901 (2011).
[50] A. Demircan, S. Amiranashvili, C. Brée, C. Mahnke, F. Mitschke, and G. Steinmeyer, Scientific Reports **2**, 850 EP (2012).